Received: 15 December 2020 | Revised: 18 April 2021 | Accepted: 2 June 2021

DOI: 10.1002/hbm.25563

RESEARCH ARTICLE

WILEY

# Visual experience modulates whole-brain connectivity dynamics: A resting-state fMRI study using the model of radiologists

Yue Wang[1] | Chenwang Jin[2] | Zhongliang Yin[3] | Hongmei Wang[2] | Ming Ji[4] | Minghao Dong[3] | Jimin Liang[1]

[1]School of Electronic Engineering, Xidian University, Shaanxi, China

[2]Department of Medical Imaging, First Affiliated Hospital of Medical College, Xi'an Jiaotong University, Shaanxi, China

[3]Engineering Research Center of Molecular and Neuro Imaging of Ministry of Education, School of Life Science and Technology, Xidian University, Shaanxi, China

[4]School of Psychology, Shaanxi Normal University, Shaanxi, China

**Correspondence**
Jimin Liang, School of Electronic Engineering, Xidian University, Xi'an, Shaanxi, 710071, China.
Email: jimleung@mail.xidian.edu.cn.

Minghao Dong, School of Life Science and Technology, Xidian University, Xi'an, Shaanxi, 710071, China.
Email: dminghao@xidian.edu.cn

**Funding information**
National Natural Science Foundation of China, Grant/Award Numbers: 61976167, U19B2030; Fundamental Research Funds for the Central Universities, Grant/Award Number: JB191206; Science Technology Projects of Xi'an, China, Grant/Award Number: 201809170CX11JC12; National Defense Basic Scientific Research Program, Grant/Award Number: JCKY2017204B102

## Abstract

Visual expertise refers to proficiency in visual recognition. It is attributed to accumulated visual experience in a specific domain and manifests in widespread neural activities that extend well beyond the visual cortex to multiple high-level brain areas. An extensive body of studies has centered on the neural mechanisms underlying a distinctive domain of visual expertise, while few studies elucidated how visual experience modulates resting-state whole-brain connectivity dynamics. The current study bridged this gap by modeling the subtle alterations in interregional spontaneous connectivity patterns with a group of superior radiological interns. Functional connectivity analysis was based on functional brain segmentation, which was derived from a data-driven clustering approach to discriminate subtle changes in connectivity dynamics. Our results showed there was radiographic visual experience accompanied with integration within brain circuits supporting visual processing and decision making, integration across brain circuits supporting high-order functions, and segregation between high-order and low-order brain functions. Also, most of these alterations were significantly correlated with individual nodule identification performance. Our results implied that visual expertise is a controlled, interactive process that develops from reciprocal interactions between the visual system and multiple top-down factors, including semantic knowledge, top-down attentional control, and task relevance, which may enhance participants' local brain functional integration to promote their acquisition of specific visual information and modulate the activity of some regions for lower-order visual feature processing to filter out nonrelevant visual details. The current findings may provide new ideas for understanding the central mechanism underlying the formation of visual expertise.

**KEYWORDS**
brain plasticity, radiologists, resting state fMRI, spontaneous dynamic interactions, visual expertise

Yue Wang and Chenwang Jin have contributed equally to this study.

## 1 | INTRODUCTION

Visual expertise refers to consistently superior performance in visual recognition for domain-specific visual recognition tasks. It is an acquired skill through at least hundreds of cases of training (Annis & Palmeri, 2019) and emerges from the reciprocal interactions between visual system and multiple top-down factors, such as semantic knowledge, attention, and task relevance (Harel, 2016). It recruits multiple systems and manifests in widespread neural activities that extend beyond a well-studied visual system to multiple high-level areas across the brain (Bar, 2003; Grill-Spector, Kourtzi, & Kanwisher, 2001).

Many expertise models have been used to study neural correlates of visual expertise and identified functional reorganization, segmentation and integration of brain networks (Kelly & Garavan, 2005). Haller et al. reported stronger activation in the right medial and middle frontal gyrus in radiologists, which is associated with a more efficient visual attention, semantic analysis and decision-making mechanism for recognizing abnormalities in X-ray images than in laypersons (Haller & Radue, 2005). Bilalić et al. observed more sensitive activation in the left fusiform gyrus (FFG) in radiologists in differentiating X-ray films from nonmedical imaging photographs than novice students, supporting the expertise view that FFG seems more likely to be connected to visual features such as holistic processing in general (Bilalic, Grottenthaler, Naegele, & Lindig, 2016). Martens et al. reported altered representations in the high-level visual cortex of ornithologists and illustrated the effects for bird expertise even extending from the frontal lobe to the lower-order visual regions, indicating that expertise is related to a combination of domain-specific and domain-general changes in neural processing (Martens, Bulthe, van Vliet, & Op de Beeck, 2018). Harel et al. compared the effects related to car expertise reported by McGugin et al. (McGugin, Gatenby, Gore, & Gauthier, 2012) and Harel et al. (Harel, Gilaie-Dotan, Malach, & Bentin, 2010), and observed common regions in the visual system and other cognitive systems, including the lingual gyrus/collateral sulcus, precuneus, and superior temporal sulcus, and these results suggest that the widespread and distributed pattern of expertise-related activity across the entire cortex is facilitated by extensive interactions between the visual system and other systems (Harel, Kravitz, & Baker, 2013). In sum, the activations of these circuits compose a neurobehavioral model of brain processes in visual expertise, consisting of visual processing, attention control, decision making and semantic analysis (Humphreys, Price, & Riddoch, 1999).

Visual expertise is fundamental to radiological expertise (Rourke, Cruikshank, Shapke, & Singhal, 2016; Samei, Krupinski, & Hendee, 2010). The superior perceptual ability of visual expertise to subtly distinguish visually similar stimuli is the primary basis for disease detection and diagnosis (Rourke et al., 2016). Radiological expertise is a domain-specific visual ability with proficiency in visual recognition and other cognitive skills (Waite et al., 2020), acquired through reviewing hundreds of cases (Nodine, Mello-Thoms, Kundel, & Weinstein, 2002; Samei et al., 2010) and involving the adaptation of perceptual mechanisms to radiographic images (Kundel, Nodine, Conant, & Weinstein, 2007). Thus, the model of radiologists is a proper entry point for exploring the mechanism of visual expertise.

In the absence of perceptual input, resting-state brain activity plays a crucial role in maintaining ongoing internal representations and is responsible for coding prior experience (Dong et al., 2014; Dong et al., 2015; Miall & Robertson, 2006). In particular, refined dynamic interactions between brain regions reflect history of repeated synchronized activation (Amad et al., 2017) and neuronal coupling (Urner, Schwarzkopf, Friston, & Rees, 2013) between brain regions in the learning process, which supports the superior behavioral performance and reflects distinctive cognitive mechanisms. To our knowledge, little attention has been paid to how visual expertise modulates connectivity patterns in resting-state brain activities. Accordingly, our current study investigated whole-brain connectivity dynamics modulated by visual expertise using the model of radiologists consisted of 20 trained superior intern radiologists (IR) and well-matched normal controls (NC) and more sensitive functional connectivity (FC) analysis to identify subtle changes in connectivity patterns. As it has been discussed beforehand, radiologists have consistently superior performance in domain-specific visual recognition tasks (Evans et al., 2011), which is supported by optimal visual processing, attention control, decision making, and semantic analysis processes, we expect to see functional integration within brain circuits supporting neurobehavioral such as visual processing and other cognitive functions, and refined connecting patterns across these circuits.

## 2 | METHODS

This study was approved by the Ethics Committee of the First Affiliated Hospital of Xi'an Jiaotong University subcommittee on Human Studies and was conducted in accordance with the Declaration of Helsinki. The detailed study design was explained to all participants before the experiment and their written informed consents were obtained.

### 2.1 | Participants

Participant recruitment was carried out among intern radiologists from the First Affiliated Hospital of Xi'an Jiaotong University and matched healthy controls from our database for visual expertise. In total, 40 healthy right-handed 4th-year undergraduates (19 males, 21 females) were recruited after a rigorous screening procedure. Twenty participants (nine males, 11 females, 23.30 ± 1.19 years old, Mean ± *SD*) underwent a 1-month visual recognition training procedure forming the IR group. The IR group consisted of medical students from the undergraduate program in national medical schools following the same training protocol as required by the same syllabus. They underwent training in the X-ray department on lung nodule recognition and reviewed 25–35 cases during their daily rotation from 8:00 a.m. to 6:00 p.m., 6 days a week. The mean duration of training was 26.1 ± 2.3 (mean ± *SD*) days, and the total number of

training cases per participant in the IR group was 763.0 ± 76.8 (Mean ± *SD*). Each of the participants in the IR group had a radiology tutor who provided clinical-based supports in each daily training. During training, participants in the IR group were required to perform a pathological analysis and fill in reports on X-ray films displayed on the monitor screen, where each case report was matched for consistency with the opinion of the radiology tutors.

On the other hand, 24th-year undergraduates (10 males, 10 females, 23.55 ± 1.12 years old, Mean ± *SD*) with no clinical experience in radiography formed the NC group. The two groups were not significantly different in age ($p = .510$, Mann–Whitney test) and were homogeneous in terms of educational level. All participants had normal or corrected-to-normal visual acuity and confirmed having no smoking habits, alcohol abuse, MRI scan restrictions, or history of mental or health disorders. Screening procedure was conducted in a face-to-face interview with all subjects from both IR and NC groups to exclude the effect of visual expertise from other known domains (e.g., cars, chess, birds, etc.). The detailed study design was explained to all participants before the experiment and their written informed consents were obtained.

## 2.2 | Behavioral measurement

Viewing conditions were controlled by excluding natural light. The experimenter started the experiment only after describing the entire procedure to the participants and making sure that the experimental protocol was fully understood. The same test bank was used for experiments in both IR and NC groups.

In order to measure the participants' perceptual ability in medical imaging, we selected 100 standard lung X-ray images from the X-ray image bank of the Department of Medical Imaging, First Affiliated Hospital of Medical College. Pathological conditions in the images were scrutinized by three senior independent radiologists with more than 10 years of experience in radiology diagnosis, and confirmed by radiological reports. In addition, the level of difficulty for judgment was also evaluated by these radiologists on a scale from 1 to 3, and the portion for each difficulty level was 55%, 30%, and 15%, respectively. Prior to testing, participants were informed that each X-ray image may contain a single nodule or no nodules, and diagnosis unrelated to lung nodules was not mentioned.

Sixty-five X-ray images, each containing only one nodule, were selected as positive cases, and 35 tumor-free X-ray images were selected as negative cases. For each testing image, participants were required to make a decision within 4 s using an in-house radiological behavioral data collection system. Their judgment of the presence or absence of nodule, confidence level of judgment, and time spent for decision-making were recorded using in-house software (Chinese Software Patent No. 2018SR036699). Standard receiver operating characteristic (ROC) curve analysis was employed to evaluate the performance of the diagnostic tests (Metz, 2006). The ROCFIT program (part of a set of curve-fitting and estimation programs called ROCKIT, available at http://www-radiology.uchicago.edu/sections) was used to produce an ROC curve after averaging the confidence intervals for each group of participants. The area under the curve (AUC) was the result of the analysis.

In addition, considering that face recognition ability is considered as inherent visual expertise, we also employed a standardized face recognition test, the Cambridge Face Memory Test (CFMT; Duchaine & Nakayama, 2006), to assess the level of face recognition ability in both IR and NC groups. The CFMT task was scored as the number of correct cases across 72 three-alternative forced-choice trials.

## 2.3 | MRI data acquisition

The imaging data in this study were collected at the First Affiliated Hospital of Medical College, Xi'an Jiaotong University, on a 3-Tesla MRI system (EXCITE, General Electric, Milwaukee, WI). A standard birdcage head coil and restraining foam pads were used to minimize head movement and reduce scanner noise.

The resting scan was recorded with a gradient-echo single-shot echo planar imaging sequence using the following parameters: scan duration = 370 s, repetition time = 2 s, field of view = 240 mm, echo time = 30 ms, matrix = 64 × 64, 32 interleaved axial slices were oriented parallel to the anterior commissure-posterior commissure line of each participant, and voxel size = 3.8 × 3.8 × 5.0 mm, no gap. Participants were asked to stay awake, keep their eyes closed, and hold their head still during the scanning process. At the end of the experiment, we confirmed that the participants did not fall asleep during the whole procedure.

In addition, for each participant, we acquired an MPRAGE T1-magnetization high resolution anatomical image (resolution: 1 × 1 × 1 mm) for co-registration using the following parameters: field of view = 256 mm, matrix = 256 × 256, repetition time = 1.9 s, echo time = 2.26 ms, flip angle = 9°, and number of slices = 176 in the sagittal orientation. Two expert radiologists screened the structural images of all participants and reported no brain abnormalities on conventional MRI.

## 2.4 | Resting-state fMRI data preprocessing

Resting-state functional MRI (rs-fMRI) data preprocessing was performed using the Data Processing Assistant for Resting-State fMRI (DPARSF) (http://www.restfmri.net/forum/DPARSF) and Statistical Parametric Mapping (SPM12) (http://www.fil.ion.ucl.ac.uk/spm) under Matlab 2009a, including: (1) discarding the first 10 volumes to avoid nonequilibrium effects; (2) slice-timing correction for acquisition delays between slices; (3) realignment to match each functional volume to the reference volume, the estimated translation and rotation parameters for each volume were confirmed to be not >1 mm and 1°, and there was no group-wise difference in frame-wise displacement (NC vs. IR = 0.048 ± 0.021 vs. 0.066 ± 0.044, Mean ± *SD*, $p = 0.242$, Mann–Whitney test); (4) regressing the effects of head motion

parameters (using the Friston's 24 head motion model), white matter, and cerebrospinal fluid signals; (5) spatial normalization and resampling of the functional images to 3 mm isotropic voxels; (6) spatially smoothing the functional images with an isotropic Gaussian kernel with a half-maximal value of 6 mm full width; (7) removing the linear trends; and (8) band-pass filtering (0.01–0.08 Hz) to reduce the effects of low-frequency drift and high-frequency noise.

## 2.5 | Brain sub-division

Predefined brain atlases used in multiple previous studies (Alaerts, Swinnen, & Wenderoth, 2016; Wang et al., 2015) summarized the functional distribution patterns of the general human brain but may not adapt well to the brain signals in specific research cases, especially those with neural plasticity modification. In this study, we compared the performance of data-driven clustering approaches and functional atlases in dividing the brain into functionally homogeneous subregions. Specifically, we selected the clustering method from five widely used clustering algorithms based on their overall accuracy to model the brain signal of interest across multiple clustering scales (Thirion, Varoquaux, Dohmatob, & Poline, 2014), including multigraph K-way spectral clustering (MKSC; Shen, Tokoglu, Papademetris, & Constable, 2013), group mean Ncut-based spatially constrained multi-class spectral clustering (MSC-mean; Craddock, James, Holtzheimer, Hu, & Mayberg, 2012), two-level Ncut-based spatially constrained multi-class spectral clustering (MSC-two-level; Craddock et al., 2012), group mean Ncut-based simple linear iterative clustering (SLIC-mean; Wang & Wang, 2016), and two-level Ncut-based simple linear iterative clustering (SLIC-two-level; Wang & Wang, 2016). The group-mean clustering strategy was accomplished by averaging the individual similarity matrices followed by submitting the average to clustering (Patel, Borsook, & Becerra, 2008), and the two-level clustering strategy by performing clustering for each individual and then conducting second-level group clustering (van den Heuvel, Mandl, & Pol, 2008). Gray matter mask (https://www.nitrc.org/projects/seecat/) with cerebellum and brainstem excluded was employed in the clustering analysis.

The above clustering methods also provided their corresponding functional atlases with multiple clustering scales obtained from the Beijing_Zang dataset (https://www.nitrc.org/projects/slic/), which usually divided the whole brain into 50 to 1000 clusters (expected number) with an interval of 50 clusters. For the comparability with these atlases, we set the expected number of clusters from 50 to 1500 with an interval of 50 clusters, and estimated the appropriate clustering scale for this study by evaluating the clustering results across the scale variants. We chose a larger upper-bound of cluster number 1500 because the spectral clustering methods (MKSC, MSC-mean, and MSC-two-level) may generate trivial solutions (i.e., empty clusters). Thus, the resultant number of clusters was less than the expected one. In the following sections, all the clustering results were evaluated using the resultant number of clusters.

### 2.5.1 | Clustering method selection

In an attempt to select a clustering method suitable for this study, we performed a functional sub-division on the rs-fMRI data using the above data-driven clustering methods and their corresponding functional atlases, respectively. We systematically evaluated the above clustering methods in terms of accuracy and reproducibility (LaConte et al., 2003). Accuracy reflects the ability of the clustering method to model the signals of interest in fMRI data, while reproducibility demonstrates the consistency of the clustering results obtained from different subsets of the dataset (Thirion et al., 2014). We first selected a clustering method from the 10 candidate methods based on the accuracy measurement of the silhouette width (Peter, 1987), and then selected an appropriate clustering scale, that is, the number of clusters, by taking into account reproducibility, cluster compactness, cluster isolation, and the results of previous studies. Reproducibility measures were not used in the selection of the clustering method because the candidate clustering algorithms in this study have different spatial constraint strategies, which would introduce an unfair comparison in the assessment of algorithm robustness. Specifically, the SLIC-mean algorithm strictly controls the numbers of clusters and gets the same number of clusters across multiple clustering operations with higher reproducibility and higher intercluster functional similarity. The MSC-mean algorithm allows the existence of empty clusters, resulting in lower intercluster functional similarity, but multiple clustering yields a different number of clusters, leading to lower reproducibility.

The silhouette width quantifies the accuracy of clustering based on the combination of cluster compactness and cluster isolation. Cluster compactness can be defined by the average of the intracluster functional similarity of all clusters. For the $k$th cluster $C_k$, the intracluster functional similarity is defined as

$$\mathrm{Intra}(k) = \frac{1}{n_k(n_k-1)} \sum_{i,j \in C_k, i \neq j} s_{ij}, k = 1,2,\cdots,K, \quad (1)$$

where $s_{ij}$ denotes the similarity between voxel $i$ and $j$ measured by the Pearson's correlation coefficient, $n_k$ denotes the number of voxels in cluster $k$, and $K$ is the total number of clusters. Cluster isolation is defined by the averaged intercluster functional similarity across all clusters. For the $k$th cluster $C_k$, its intercluster functional similarity is defined as

$$\mathrm{Inter}(k) = \frac{1}{n_k(N-n_k)} \sum_{i \in C_k, j \notin C_k} s_{ij}, \quad (2)$$

where $N$ is the total number of voxels. The Silhouette width can be calculated by (Peter, 1987)

$$\mathrm{Silhouette} = \frac{1}{K} \sum_{k=1}^{K} \frac{\mathrm{Intra}(k) - \mathrm{Inter}(k)}{\max[\mathrm{Intra}(k), \mathrm{Inter}(k)]}. \quad (3)$$

Taking silhouette width as a measure of accuracy, the best performance of the above clustering methods was used for the following analysis.

### 2.5.2 | Clustering scale estimation

Subsequently, on the basis of the selected clustering method, we estimated the clustering scale appropriate for this study by taking into account the clustering reproducibility, cluster compactness, cluster isolation, and reports of previous studies on radiologists. The clustering scale was usually represented as the size of the cluster (Parisot, Arslan, Passerat-Palmbach, Wells, & Rueckert, 2016), which was closely related to the number of clusters that a clustering method used to partition the data. In this article, we do not strictly distinguish between these two expressions.

For the clustering reproducibility measurement, all participants were split equally into two subgroups, with each subgroup constructed with 10 randomly selected participants from the IR and NC groups, respectively. The subgroup splitting procedure was repeated 10 times for the credibility of evaluation (Wang & Wang, 2016). For each subgroup split, two subgroups were clustered separately, with an expected number of clusters from 50 to 1500 in steps of 50. We employed the adjusted rand index (ARI) and adjusted mutual information (AMI; Nguyen, Epps, & Bailey, 2010) metrics to measure the reproducibility of each split and to estimate the clustering scale appropriate for this study. The ARI measures the similarity between two clustering results, which is invariant to the permutation of cluster labels. The AMI measures the mutual information of two discrete assignments of voxels to clusters. The higher the value of ARI or AMI, the better the reproducibility of the clustering method.

Since the ARI and AMI typically fluctuate with the clustering scales (Thirion et al., 2014), we selected the numbers of clusters with local maximums of ARI or AMI as candidates and estimated the expected clustering scale (in terms of the number of clusters, denoted as $\hat{K}$) for this study through comprehensive consideration of cluster compactness, cluster isolation, and reports of previous radiologist studies. On the one hand, we desire a sufficiently large number of regions to guarantee that they were functionally homogeneous and adequately represent the connectivity information presented in the rs-fMRI data. On the other hand, too many regions would make statistical inference challenging, leading to an explosion in computational complexity and interfere with the interpretability of the observed connections (Varoquaux & Craddock, 2013). The size of activated brain regions reported in previous radiologist studies may provide a rational basis for our choice of clustering scale. We expect that the cluster size should be appropriately small to avoid obliterating the radiographic visual experience effect, while allowing good interpretability of the results. Choosing a cluster size similar to the size of previously reported activation areas may better satisfy both of these requirements.

Once the appropriate clustering scale was obtained, the clustering method was performed again with a cluster number set larger than the expected $\hat{K}$. The resultant number of clusters is denoted as $K$. Afterwards, the intrinsic brain activity signal was obtained by averaging the rs-fMRI BOLD signal series across voxels within each cluster. For each participant, the brain activity can be expressed as $Z_p \in R^{K\times T}$, where $p = 1,2,\cdots,P$ is the index of participant, $p = 40$ is the number of participants, and $T = 175$ is the number of slices.

## 2.6 | Functional connectivity analysis

Functional connectivity between brain regions can be measured by calculating the correlation matrix of the intrinsic brain activity signals (i.e., each row of $Z_p$). Since the correlation matrix captures a large amount of sampling noise and inherent randomness that arises in the estimation of correlations between short time series, the correlation matrix estimator is a good alternative for recovering the connectivity structure (Varoquaux, Gramfort, Poline, & Thirion, 2010). In the current study, the correlation matrix $X_p^c \in R^{K\times K}$ for each participant was generated by Ledoit–Wolf shrinkage estimation (Ledoit & Wolf, 2004). Noteworthy, for the problem of recovering the functional connectivity structure, sparse inverse covariance estimators have been found to be efficient, which could capture the effects of other regions for the standard correlation between two regions (Varoquaux & Craddock, 2013). In this study, we also calculated the inverse covariance matrix $X_p^m \in R^{K\times K}$ for each participant using the Graphical Lasso estimation (Friedman, Hastie, & Tibshirani, 2008).

The above correlation matrix and inverse covariance matrix carried a lot of information on the functional structure of the brain: the correlation matrix captures the large-scale functional network, and the inverse covariance matrix captures partial correlations that can be regarded as the backbone or core of the brain networks. Since the spurious background associations between different regions across participants often made FC analysis challenging (Varoquaux & Craddock, 2013), a strategy for second-level analysis was proposed to disentangle the background association effects from the intrinsic connectivity and give unstructured residuals (Varoquaux, Baronnet, Kleinschmidt, Fillard, & Thirion, 2010). We performed a statistical test for FC analysis on the residuals of a parametrization intermediate (Varoquaux, Baronnet, Kleinschmidt, Fillard, & Thirion, 2010) between the correlation matrix $X_p^c \in R^{K\times K}$ generated by Ledoit–Wolf shrinkage estimation (Ledoit & Wolf, 2004) and the inverse covariance matrix $X_p^m \in R^{K\times K}$ produced by Graphical Lasso estimation (Friedman et al., 2008). The correlation matrix $X_p^c$ can be expressed as composed of the nonspecific intrinsic matrix $X_p^m$ and the participant-specific effect matrix $dX_p^c$ (Varoquaux, Baronnet, Kleinschmidt, Fillard, & Thirion, 2010):

$$X_p^c = X_p^m + dX_p^c. \tag{4}$$

Equation (4) can be approximated as:

$$X_p^c \approx X_p^{m^{\frac{1}{2}}}\left(I_K + dX_p^c\right)X_p^{m^{\frac{1}{2}}}, \tag{5}$$

where $I_K$ is an identity matrix with the same dimensions as the correlation matrix. Thus, the participant-specific effect matrix $dX_p^c$ can be approximated by:

$$dX_p^c \approx X_p^{m\,-\frac{1}{2}} X_p^c X_p^{m\,-\frac{1}{2}} - I_K. \quad (6)$$

The above method decouples the participant-specific effects (i.e., actual connections) distributed over the correlation matrices from background noises (i.e., spurious connections) carried by the inverse covariance matrices (Varoquaux & Craddock, 2013). Thereafter, Fisher's $z$ transformation was applied to each participant-specific effect matrix $dX_p^c$. For intergroup FC comparisons, the effect of frame-wise displacement (FD) and face recognition ability (i.e., the CFMT scores) were regressed out, and a nonparametric permutation test was performed: calculate the difference between the mean values of the IR and NC groups, denoted $\bar{x}$, regroup the samples and calculate the difference between means of the two groups, denoted $\bar{x}_i$, repeat the regrouping operation 10,000 times and take the proportion of $\bar{x}_i > \bar{x}$ in the 10,000 iterations as the uncorrected $p$ value, and then control the false discovery rate (FDR) $p < .05$. In addition, a correlation analysis was conducted to examine the relationship between the interregional FC calculated using the averaged BOLD signals within subregions and lung nodule identification performance indexed by the area under the receiver operating characteristic curve for lung nodule identification. The pipeline of the data analysis in this study is illustrated in Figure 1.

In addition, in order to evaluate the power of the results, we conducted a post-hoc analysis with the significant level set to .05 and sample number set to 20, and the power of each reported FC was calculated. In addition, a prior analysis was conducted to evaluate the effect sample size for each reported FC with the power set to 0.95. These power analyses were performed using the GPower software (v3.1) (Faul, Erdfelder, Lang, & Buchner, 2007).

## 3 | RESULTS

### 3.1 | Results of behavior tests

Behavior feature of IR and NC groups are summarized in Figure 2. The two groups were not significantly different in CFMT scores ($p = .174$, Mann–Whitney test). In the behavioral test of lung nodule

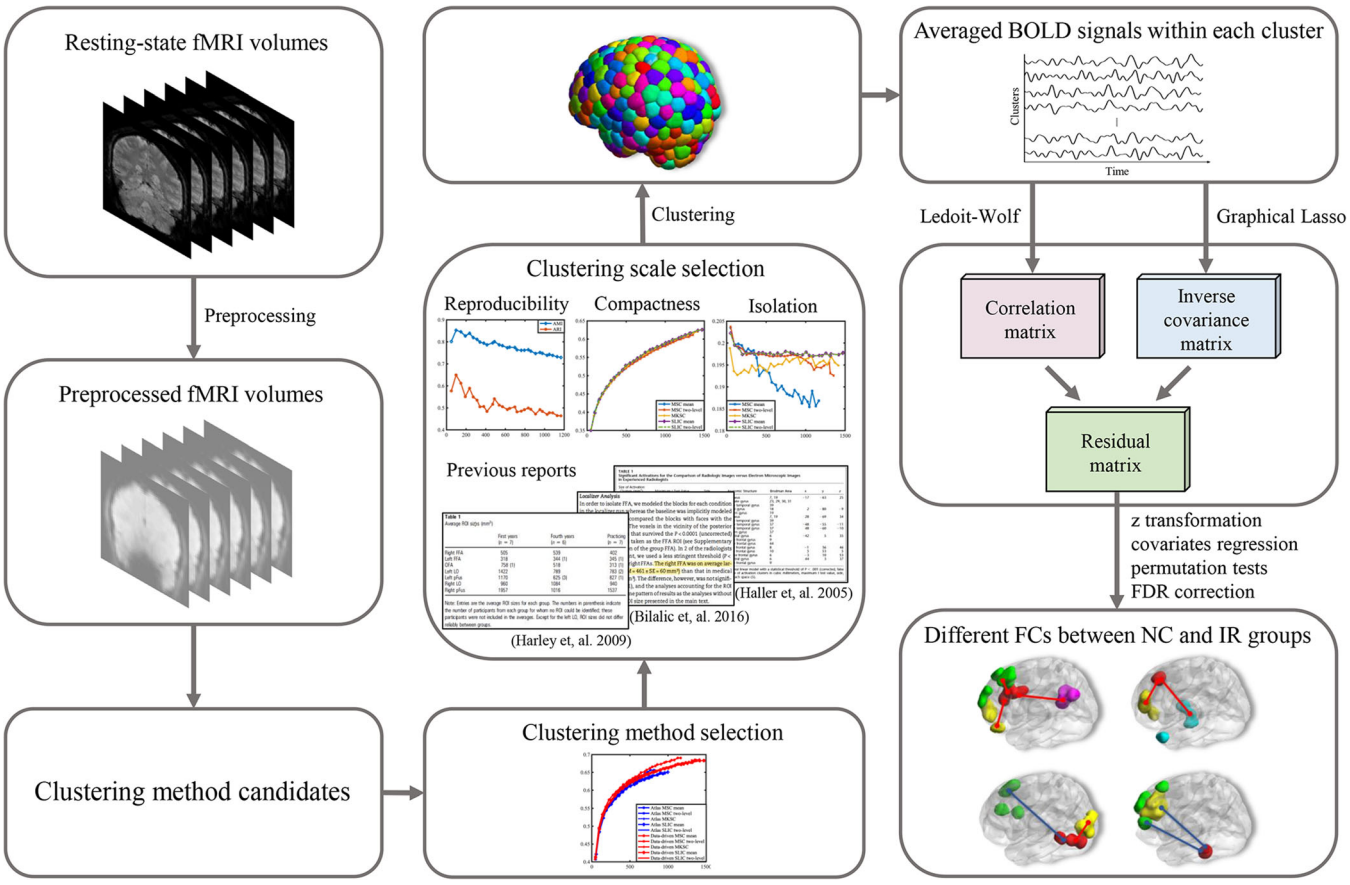


**FIGURE 1** Pipeline of the whole-brain functional connectivity analysis of rs-fMRI data. The rs-fMRI data were preprocessed and divided into subregions using a carefully selected clustering algorithm and scale for further analysis. Functional connectivity analysis was performed on the residuals of a parametrization intermediate between the correlation matrix generated by the Ledoit–Wolf shrinkage estimation and the inverse covariance matrix produced by Graphical Lasso estimation. Then, functional connections with differences between intern radiologists and normal control groups were obtained after Fisher's $z$ transformation, covariates regression, nonparametric permutation test, and false discovery rate correction

recognition, the AUC of the 1-month trained IR group was significantly higher than that of the NC group (IR group: mean = 0.80, *SD* = 0.04 vs. NC group: mean = 0.53, *SD* = 0.02, $p < .001$, Mann–Whitney test), indicating a better nodule recognition ability in the trained group. For the IR group, the AUC of ROC in nodule recognition fell in the interval of 0.73–0.86, which indicated that our experimental design was reliable, according to the guidelines for designing proper behavioral assessment for radiological performance (Samei et al., 2010). The 1-month visual recognition training in the X-ray department had considerably improved the lung nodule identification performance of participants in the IR group, as demonstrated by the comments of radiology tutors. Moreover, there was no significant difference in the score of CFMT between the IR and NC groups (IR group: mean = 56.8, *SD* = 5.5 vs. NC group: mean = 59.2, *SD* = 5.2, $p = .174$, Mann–Whitney test), which demonstrated that the two groups had similar face recognition abilities.

## 3.2 | Results of the clustering method selection

The silhouette width of the results of the brain sub-division is illustrated in Figure 3a, with the data-driven generated results in red and the atlas generated results in blue. The data-driven methods show an overall higher silhouette width, confirming our anticipation that data-driven methods were better adapted to the brain signals in this study than predefined functional atlases. The MSC-mean method had the highest silhouette width with comparable intracluster homogeneity (Figure 3b) and better intercluster isolation (Figure 3c) than other methods. Therefore, the MSC-mean method was adopted to divide the brain into sub-regions in the following analysis.

## 3.3 | Results of the clustering scale estimation

For clustering reproducibility measurement (Figure 3d, average of 10 subgroup partitions), both ARI and AMI reached prominent local maxima when the expected number of clusters were set to 100, 250, and 600, and the whole brain was divided into approximately 98, 235, and 489 clusters, respectively. The number of clusters at the local maxima of AMI and ARI indicated that some stable features could be captured when the whole brain was divided into these numbers of clusters (Thirion et al., 2014). Then, we selected the expected cluster scale from the above three candidate numbers of clusters by taking into account the following factors. First, the size of activated brain regions reported in previous radiologist studies (Bilalic et al., 2016; Haller & Radue, 2005; Harley et al., 2009) was mostly found in the range of 604 to 7046 $mm^3$ (mean = 2,127 $mm^3$, *SD* = 1744 $mm^3$, median = 1580 $mm^3$, after removing the top five and bottom five outliers), while the region sizes corresponding to 98, 235, and 489 clusters were approximately 18,000, 7500, and 3600 $mm^3$, respectively. Among the above three candidates, dividing the whole brain into the scale (i.e., 489 clusters) that was similar to the previously reported scale of activation areas could better satisfy the requirements of avoiding the obliteration of radiographic visual experience effects and have good interpretability of the results. Second, the clustering scale of 489 clusters produced significantly better cluster compactness and cluster isolation than 98 or 235 clusters (Figure 3b,c), indicating that the ability of the clustering method to model the signals of interest was strongest when dividing the whole brain into approximately 489 clusters. Third, as the number of sub-regions increases from 400 to 600 (Figure 3d), the algorithm's reproducibility indices were monotonically increasing and decreasing before and after reaching the local maxima at 489, respectively. The absence of abrupt changes in the reproducibility index within this interval of the number of sub-regions makes our choice of a cluster number around 489 clusters more reliable.

Taking all these factors into account, we set the expected number of clusters for the MSC-mean method to 600 (>489 because of the presence of trivial solutions) and eventually divided the whole brain into 512 sub-regions.

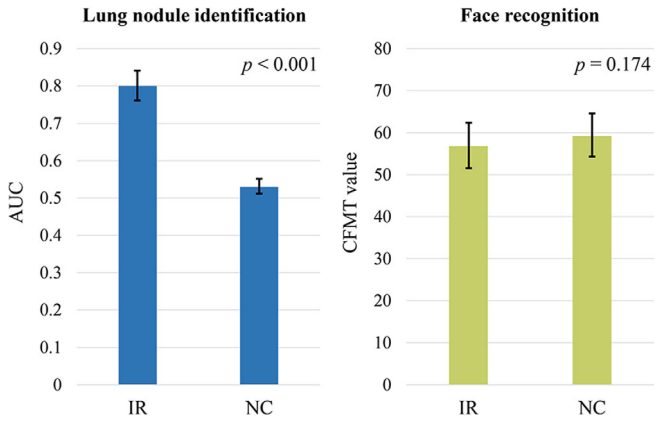


**FIGURE 2** Individual performance of lung nodule identification and face recognition. The error bars denote the standard deviation of the AUC or values in the Cambridge Face Memory Test for each group. The AUC is the area under the receiver operating characteristic curve for lung nodule identification

## 3.4 | Results of functional connectivity and correlation analysis

In the cluster-based whole-brain FC analysis, significant intergroup differences in temporal synchronism were observed: (1) between cingulate gyri and frontal areas, precuneus (PCUN), and temporal areas, (2) between the lingual gyrus (LING) and occipital and frontal areas, and (3) between the fusiform gyrus (FFG), cingulate gyri, and frontal areas.

The results of the FC and correlation analysis are presented in Table 1, which lists the name of brain regions and their corresponding hemisphere (Hem), Brodmann area (BA), MNI coordinates, the Spearman's correlation coefficient (*r*) with a significant correlation ($p < .05$, FDR corrected) between its associated FC and visual recognition accuracy, and the power ($1 - \beta$) and effect sample number in each group (*N*) evaluated by post-hoc and a priori analyses. The names of brain regions in this study were defined according to the automated anatomical labeling (AAL) template (Tzourio-Mazoyer et al., 2002). Among the 27 connections reported with significant

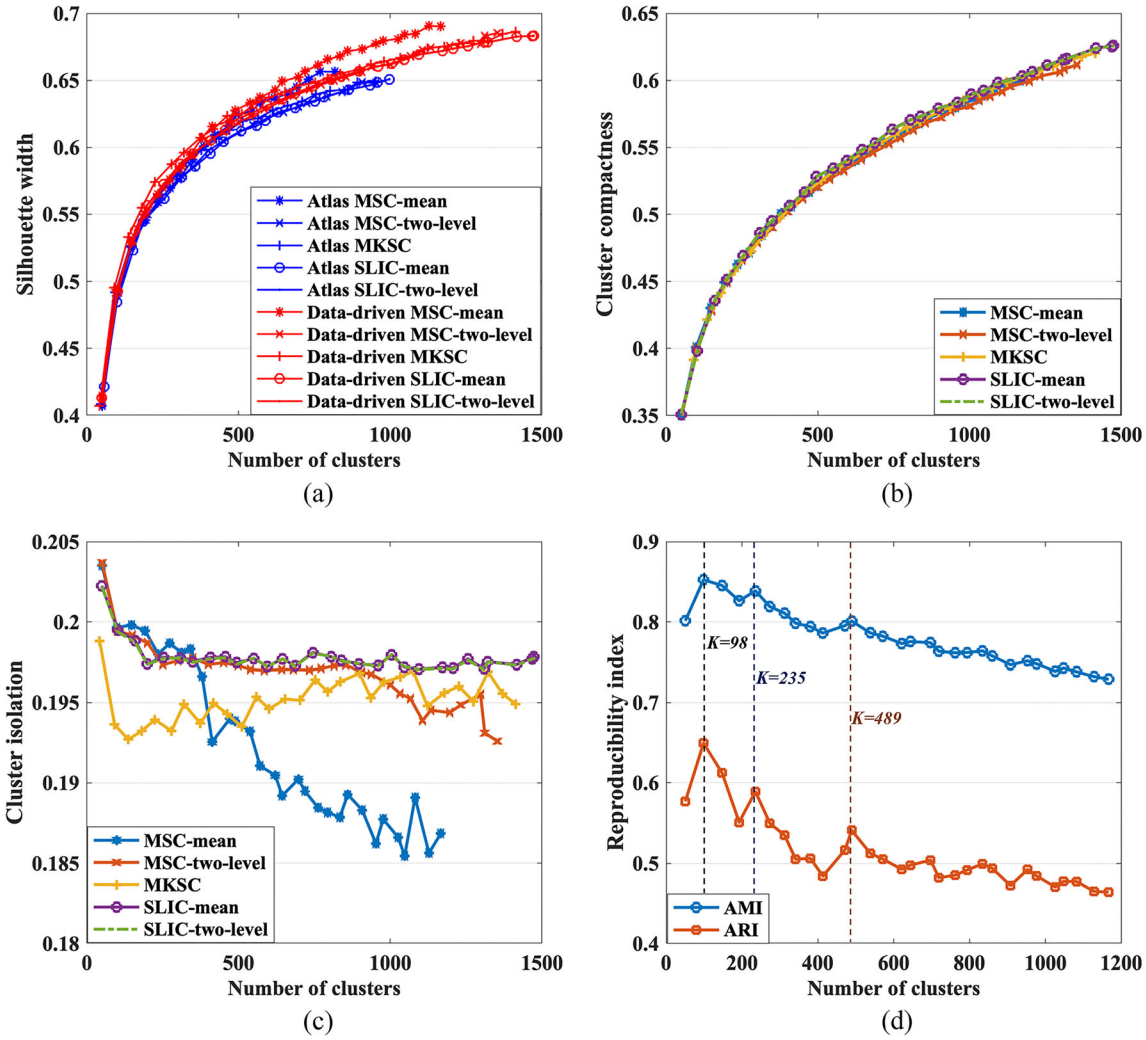


**FIGURE 3** Results of clustering performance evaluation. (a) Silhouette width of data-driven clustering methods and predefined functional atlases. (b) Cluster compactness of the data-driven clustering methods across multiple clustering scales. (c) Cluster isolation of the data-driven clustering methods across multiple clustering scales. (d) The adjusted mutual information and adjusted rand index of the MSC-mean method across different clustering scales

group-wise FC difference, seven of which were found to have insufficient statistical power due to an inadequate sample size as shown in the last two columns of Table 1. Although this does not affect the interpretation of the results, we do suggest that further studies with larger samples are encouraged to repeat the current findings.

Specifically, a significant higher temporal synchronism ($p < .001$, permutation test, FDR corrected) was observed in the IR group between the bilateral dorsal anterior cingulate gyrus (ACGdor; 5, 30, 18, BA24) and (1) superior frontal gyrus (SFG), including the bilateral medial SFG (SFGmed) and left dorsolateral SFG (SFGdor), (2) orbital frontal gyrus (OFG), including bilateral superior OFG (OFGsup) and left inferior OFG (OFGinf), and (3) bilateral PCUN; between the right median cingulate gyri (MCG; 10, 34, 34, BA32) and (1) bilateral middle temporal pole (TPOmid), and (2) frontal areas, including the left SFGmed and right OFGsup; and between the left LING and bilateral occipital and occipital-adjacent regions, including the superior occipital gyrus (SOG), left calcarine fissure (CAL), and left cuneus (CUN).

In contrast, significantly lower temporal synchrony ($p < .001$, permutation test, FDR corrected) was observed in the IR group between the left LING (−28, −61, 0, BA19) and right frontal areas, including the right middle frontal gyrus (MFG), right middle OFG (OFGmid), and right OFGinf. In addition, significantly lower temporal synchrony ($p < .001$, permutation test, FDR corrected) was observed in the IR group between the left FFG (−42, −53, −15, BA37) and bilateral ACGdor, right MCG, and frontal areas, including the right SFGdor, left medial orbital superior frontal gyrus (OFGsupmed), and left SFGmed. Most aforementioned brain regions were also observed in previous task-state radiographic visual expertise studies (Bilalic et al., 2016; Haller & Radue, 2005; Melo et al., 2011).

In addition, we stated that the differences of interregional FC were not likely to be contributed by other categories of visual expertise, since the expertise in other domains were either excluded from participant inclusion or controlled by additional behavioral tests (i.e., face recognition expertise). Normally, the perceptual ability of radiographic

**TABLE 1** Results of functional connectivity and correlation analysis

| | | | Coordinates | | | | | | Coordinates | | | | | |
|---|---|---|---|---|---|---|---|---|---|---|---|---|---|---|
| Name | Hem | BA | *x* | *y* | *z* | Name | Hem | BA | *x* | *y* | *z* | *r* | $1-\beta$ | *N* |
| ACG | R | 32 | 10 | 36 | 16 | Medial SFG | R | 9 | 12 | 51 | 41 | | 0.962 | 19 |
| | L/R | | 0 | 10 | 26 | Medial SFG | L | 8 | -5 | 28 | 46 | 0.542 | 0.965 | 19 |
| | R | 32 | 10 | 36 | 16 | Dorsolateral SFG[a] | L | 10 | −20 | 59 | 20 | | 0.885 | 26 |
| | R | 32 | 10 | 36 | 16 | Dorsolateral SFG[a] | L | 8 | −20 | 28 | 55 | | 0.924 | 23 |
| | L/R | | 0 | 10 | 26 | Superior OFG | R | 11 | 10 | 60 | −19 | 0.323 | 0.974 | 18 |
| | L/R | | 0 | 10 | 26 | Superior OFG[a] | L | 11 | −8 | 58 | −22 | | 0.944 | 21 |
| | R | 32 | 10 | 36 | 16 | Inferior OFG | L | 47 | −42 | 31 | −16 | | 0.951 | 20 |
| | R | 11 | 9 | 39 | 2 | PCUN | R | | 12 | −56 | 34 | 0.345 | 0.969 | 18 |
| | R | 32 | 10 | 36 | 16 | PCUN[a] | L | | −9 | −59 | 29 | | 0.806 | 32 |
| MCG | R | 32 | 10 | 34 | 34 | Middle TPO | L | 21 | −51 | 12 | −26 | 0.316 | 0.956 | 20 |
| | R | 32 | 10 | 34 | 34 | Middle TPO | R | 21 | 55 | 9 | −33 | | 0.959 | 19 |
| | R | 32 | 10 | 34 | 34 | Medial SFG | L | 10 | −15 | 50 | 8 | | 0.982 | 16 |
| | R | 32 | 10 | 34 | 34 | Superior OFG | R | 11 | 15 | 47 | −23 | | 0.978 | 17 |
| LING | L | 19 | −28 | −61 | 0 | MFG[b] | R | 46 | 36 | 47 | 29 | −0.408 | 0.968 | 19 |
| | L | 19 | −28 | −61 | 0 | Middle OFG[b] | R | 47 | 29 | 50 | −3 | −0.352 | 0.990 | 15 |
| | L | 19 | −28 | −61 | 0 | Inferior OFG[b] | R | 47 | 36 | 28 | −6 | −0.326 | 0.962 | 19 |
| | L | 19 | −28 | −61 | 0 | SOG[a] | R | 17 | 15 | −93 | 22 | | 0.852 | 29 |
| | L | 19 | −28 | −61 | 0 | SOG[a] | L | 17 | −15 | −93 | 22 | | 0.902 | 25 |
| | L | 19 | −28 | −61 | 0 | CAL | L | 17 | −6 | −83 | 8 | 0.422 | 0.999 | 11 |
| | L | 19 | −28 | −61 | 0 | CUN | L | 17 | −6 | −94 | 19 | 0.430 | 0.993 | 14 |
| FFG | L | 37 | −42 | −53 | −15 | Dorsal ACG[b] | R | 32 | 10 | 36 | 16 | −0.328 | 0.974 | 18 |
| | L | 37 | −42 | −53 | −15 | Dorsal ACG[b] | L | 32 | −4 | 40 | 16 | | 0.970 | 18 |
| | L | 37 | −42 | −53 | −15 | MCG[b] | R | 32 | 10 | 35 | 35 | −0.401 | 0.992 | 14 |
| | L | 37 | −42 | −53 | −15 | Dorsal SFG[b] | R | 10 | 17 | 55 | 7 | | 0.958 | 20 |
| | L | 37 | −42 | −53 | −15 | OFGsupmed[b] | R | 10 | −8 | 53 | −2 | −0.403 | 0.976 | 17 |
| | L | 37 | −42 | −53 | −15 | Medial SFG[a,b] | L | 8 | −8 | 28 | 58 | | 0.949 | 21 |
| | L | 37 | −42 | −53 | −15 | Medial SFG[b] | L | 9 | −8 | 53 | 36 | | 0.991 | 15 |

Abbreviations: BA, Brodmann's area; Hem, hemisphere; *N*, the effect sample number in each group evaluated by a prior analysis; *r*, Spearman' correlation coefficient; $1-\beta$, the power evaluated by post-hoc analysis.

[a]Insufficient statistical power due to an inadequate sample size, otherwise sufficient.

[b]Weakened functional connectivity in the IR group, otherwise enhanced.

visual recognition is obtained by reviewing hundreds of cases (Nodine et al., 2002; Samei et al., 2010). We conducted a correlation analysis between FC and the number of training cases within the IR group to test the homogeneity of the training sample size and found no significant correlation between them, indicating that the number of cases participants reviewed do not affect the FC of the IR group. In other words, the amount of training was homogeneous in the IR group.

## 4 | DISCUSSION

The visual expertise model of radiologists is rare but important (Bilalic et al., 2016; Haller & Radue, 2005). Radiological expertise is acquired through reviewing hundreds of cases (Nodine et al., 2002; Samei et al., 2010). It is a fundamental skill whose key ability is to identify subtle abnormalities on an initial global analysis of the retinal image (Myles-Worsley, Johnston, & Simons, 1998; Wallis & Bulthoff, 1999). Numerous functional neuroimaging studies investigated the brain dynamics involved in visual expertise. These studies have revealed an involvement of widespread brain regions supporting radiologists' superior ability in visual recognition, such as frontal gyrus, fusiform gyrus, lingual gyrus/collateral sulcus, precuneus, and superior temporal sulcus (Bilalic et al., 2016; Haller & Radue, 2005; Harel et al., 2010). The activations of these circuits compose a neurobehavioral model of brain processes in visual expertise, consisting of visual processing, memory, and semantic analysis and refined connecting patterns across these circuits. The current study investigated how visual experience modulates resting-state whole-brain connectivity dynamics using the expertise model of radiologists and a more sensitive functional connectivity (FC) analysis to identify subtle changes

in connectivity patterns. Radiologists have superior perceptual ability in distinguishing visually similar stimuli (Samei et al., 2010), which is supported by a complex brain process of visual processing, attention control, decision making and semantic analysis. Our results illustrated integration across brain circuits supporting high-order functions, that is, decision making and attention control as well as decision making and semantic processing (Figure 4), and integration within brain circuits supporting visual processing and decision making (Figure 4). Interestingly, we also found segregation between high-order cognitive and low-order perceptual brain networks, such as visual processing and attention control as well as visual processing and decision making (Figure 4).

## 4.1 | Integration within brain circuits supporting visual processing and decision making

### 4.1.1 | Higher coherence between regions for visual perception

Compared with the NC group, the IR group has higher coherence within FCs responsible for visual processing. Specifically, significant higher FCs were observed between the left LING (belongs to visual area V2) and the sub-regions of the primary visual cortex (visual area V1) including the bilateral SOG (BA17/18), left CAL, and left CUN (collectively referred to as V1 [Ji et al., 2019] in Figure 4). Visual expertise is an acquired skill through learning hundreds of cases with domain-specific visual features (Annis & Palmeri, 2019). The acquisition of expert knowledge may be accompanied by an increase in the cohesion of visual processing functions. In the process of visual learning, the neural computation in the human brain remodels the sensory responses (Ji et al., 2019), which makes the brain more perceptive and makes it easier for subjects to recognize specific features in images (Haller & Radue, 2005). The ventral visual stream is thought to be a basis of visual recognition (Ungerleider & Haxby, 1994), which starts with V1, relays to V2, and finally reaches the inferior temporal cortex (Song et al., 2017). Thus, increases in coherence within the ventral visual stream should be associated with enhanced visual abilities.

In this study, a significant higher FC was observed in the IR group between regions belonging to V2 and V1 within the ventral visual stream. LING belonging to visual area V2 is a brain region for early visual processing that has been found to be associated with the encoding of image features (Machielsen, Rombouts, Barkhof, Scheltens, & Witter, 2000) and skill learning such as word learning

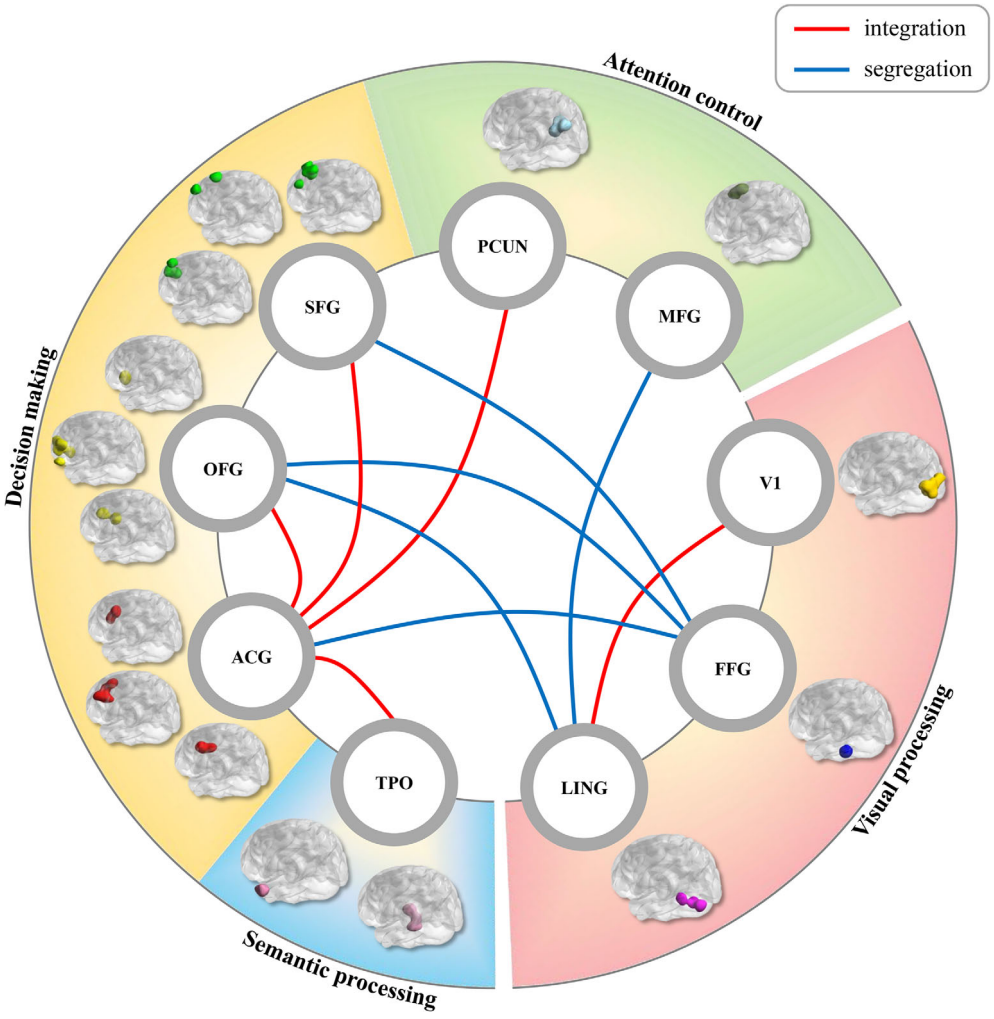


**FIGURE 4** Altered functional connectivity with their possible corresponding functional integration (red lines) or segregation (blue lines) in the IR group. The locations of ACG, SFG, OFG, and TPO are represented by multiple images for two reasons: (1) the sub-regions of TPO are disconnected and located in different hemispheres; and (2) changed functional connections in the ACG, SFG, or OFG were observed in different sub-regions. Detailed brain region connections are shown in Figures S1–S3

(Marcotte & Ansaldo, 2014), associative visual learning (Ji et al., 2019), perceptual learning (Liu et al., 2016), and always to be activated among visual experts according to the evidence from meta-analysis (Neumann, Lotze, & Eickhoff, 2016). In addition, LING has been observed to be co-activated across the habituation and acquisition phases of associative visual learning with CAL and CUN belonging to visual area V1 (Ji et al., 2019), and among presbyopia subjects with improved near-reading abilities after perceptual learning with CUN belonging to V1 (Liu et al., 2016). Evidence on human vision suggested that functional integration in the ventral visual stream provides the basis for efficient processing of visual information, where V1 provides critical input to V2, and V2 modulates the information transmitted through V1 (Friston, Ungerleider, Jezzard, & Turner, 1995). In the present study, the FC between LING and CAL and between LING and CUN were significantly correlated with the accuracy of lung nodule identification in participants, indicating that the higher FC between V1 and V2 was associated with the improvement of individual behavioral performance. Therefore, we speculate that as radiographic visual learning progresses, participants will become familiar with lung nodule-specific visual features, which may facilitate the joint activation of lower-order visual areas and allow visual perceptual processing of nodule-specific features to be more efficient.

#### 4.1.2 | Higher coherence between regions for decision-making

Compared with the NC group, the IR group has higher coherence within FCs responsible for decision-making. Specifically, significant higher FCs were observed between regions for decision-making: between ACGdor and SFG, and between ACGdor and OFG in the IR group. Decision-making is the process of flexibly aligning cognitive and sensorimotor operations based on an assessment of potential costs (Lee, Rushworth, Walton, Watanabe, & Sakagami, 2007), which is essential in expert visual processing (Donovan & Litchfield, 2013; Vila-Maldonado, Abellán, Sáez-Gallego, García-López, & Contreras, 2014). The connectivity between brain regions within the decision-making function increases with visual training (Bueicheku, Miro-Padilla, & Avila, 2019), which suggests that the acquisition of visual expertise is accompanied by an increase in cohesion within the decision-making function.

Significantly higher FCs were observed in the IR group between brain regions within the decision-making function: between ACGdor and frontal areas including SFG and OFG. ACG is located strategically in the central place for processing top-down and bottom-up stimuli and assigns appropriate control to other brain regions (Pavlovic, Pavlovic, & Lackovic, 2009). It appears to be especially involved when effort is needed to carry out tasks, such as during early learning or problem solving (Allman, Hakeem, Erwin, Nimchinsky, & Hof, 2001). The functions of ACG could be summarized into two major categories: 1) conflict detection, such as error detection, task anticipation, motivation, and modulation of emotional processes (Bush, Luu, & Posner, 2000; Nieuwenhuis, Riddeerinkhof, Blow, Band, & Kok, 2001; Posner & Digirolamo, 1998); 2) cognitive control, such as decision-making and reward-based learning (Lee et al., 2007). The dorsal part of ACG, that is, the ACGdor, is the central station on control distribution (Posner & Digirolamo, 1998), which is contained within an extensive network of cortical regions, including the SFG and OFG, that serve as neural substrates for decision-making (Bush et al., 2000; Miller, 2000; Paus, 2001; Posner & Raichle, 1995). The joint activation of ACG and SFG (Roelofs, van Turennout, & Coles, 2006), and the joint activation of ACG and OFG have been observed in decision-making (Lee et al., 2007).

In this study, we tended to summarize the function of ACG as decision-making by comprehensively considering the theory of the model of radiologists and the function of FCs involved in the ACG. According to the model of radiologists, the cognitive process of radiographic image interpretation may more or less involve the participation of functions of conflict detection and decision-making (Nodine, Kundel, Lauver, & Toto, 1996). While the FC between ACG and SFG and between ACG and OFG have significant group-wise differences generally related with decision-making. Therefore, we prefer to summarize the function of ACG as decision-making in this study. In addition, the strength of FC between ACGdor and SFG was found in relation to the experience of visual learning in both task and resting states (Bueicheku et al., 2019). In this study, the FCs between ACGdor and SFG and between ACGdor and OFG were significantly correlated with subject's lung nodule identification accuracy, suggesting that the higher FC between brain regions for decision-making was associated with the improvement of individual behavioral performance. Given that the coordinated activation of cortical regions during behavior shapes the organizational pattern of correlated spontaneous activity at rest (Lewisa, Baldassarre, Committeri, Romani, & Corbetta, 2009), we speculate that the higher FC between brain regions for decision-making may be attributed to the co-activation of ACG, SFG, and OFG during radiographic visual recognition learning. These results imply a better communication mechanism of the decision-making system built as radiographic visual learning proceeds.

### 4.2 | Integration across brain circuits supporting high-order functions

Our results elucidated that training in radiographic visual recognition increased association between high-level cognition functions, such as decision-making and top-down attention control, decision-making and semantic processing. In details, the FC were significantly higher in the IR group between ACGdor and PCUN, and between ACGdor and TPO.

Top-down attention control is the process of activating, regulating, and monitoring how information is received and processed, and is embodied in multiple processes such attention guidance, focus shifting, environmental monitoring, and stimuli context assessment (Cavanna & Trimble, 2006; Kawashima, Roland, & O'Sullivan, 1995; Vogt & Derbyshire, 2009; Wagner, Shannon, Kahn, & Buckner, 2005;

Wenderoth, Debaere, Sunaert, & Swinnen, 2015). It has a pivotal role in the reading of domain-specific visual information such as radiographic images, which may be attracted to a particular feature and then compared to the previously learned reference images (Haller & Radue, 2005; Harley et al., 2009). The top-down attention control network has rich functional interaction with the decision-making network in the process of visual perception and recognition (Wang, Zhang, Klein, Levi, & Yu, 2014; Xiao et al., 2008). The increase of functional interaction strength between the two networks was closely associated with improved visual ability acquired through learning (Niu et al., 2014).

In this study, higher FC was observed in the IR group between regions for top-down attention control (i.e., the PCUN) and decision-making (i.e., the ACG). PCUN is a focal area of attention organization, where information from various brain regions is integrated (Lin, Hasson, Jovicich, & Robinson, 2011), and is involved in various attentional processes such as attention directing (Kawashima et al., 1995), focus shifting (Cavanna & Trimble, 2006; Wenderoth et al., 2015), environment monitoring, and stimuli context assessing (Vogt & Derbyshire, 2009; Wagner et al., 2005). Moreover, PCUN is closely related to visual learning, such as associative visual learning (Ji et al., 2019) and word learning (Marcotte & Ansaldo, 2014). In addition, PCUN has been observed to be co-activated with ACG under a variety of cognitive processes such as in tasks that require goal-directed attention modulation, integration, and shifting (Wenderoth et al., 2015), and during the acquisition phase of associative visual learning (Ji et al., 2019). In this study, the FC between PCUN and ACG was also positively correlated with participants' lung nodule identification performance. These results imply a more effective functional interaction mechanism between attention control and decision-making functions that enabled the trained participants to locate a specific combination of lung nodule-specific visual features and show higher nodule identification accuracy.

Semantic processing is a process to store and discern subtle similarities and differences of concepts, which is recruited during tasks that require concept recognition or comparison such as identifying familiar faces and scenes, or identifying voices (Nakamura et al., 2000; Nakamura et al., 2001). Semantic discrimination is closely interrelated with attention control and decision-making systems (Niu et al., 2014), and is indispensable for visual recognition (Vandenberghe, Price, Wise, Josephs, & Frackowiak, 1996) and visual learning (de Hoz, Knox, & Morris, 2003; Roland, Gulyas, Seitz, Bohm, & Stone-Elander, 1990). Moreover, evidence from visual studies showed that brain areas that are related to decision-making are involved in semantic discrimination (Gold & Shadlen, 2007), which implied the vital role of interaction between semantic processing and decision-making for visual processing. Therefore, we speculate that learning to discriminate sophisticated visual features may result in an enhancement in functional interaction between brain systems of semantic processing and decision-making.

FC between regions for semantic processing (i.e., the TPO) and decision-making (i.e., the ACG) were significantly higher in the IR group than in the NC group. TPO is an essential member of the mentalizing (i.e., theory of mind) system and is concerned with generating a broader semantic and emotional context for the materials being processed based on the experience (Frith & Frith, 2003). TPO is often activated in tasks that require semantic comparison or discrimination such as comparing sentences with unrelated strings of words (Vandenberghe, Nobre, & Price, 2002), examining highly coherent versus less coherent narratives (Maguire, Frith, & Morris, 1999), and probing knowledge of associations between concepts and the visual attributes of those concepts (Vandenberghe et al., 1996). Besides, TPO is strongly associated with prior experience of skill learning. Evidence from magneto-encephalographic source localization, corroborated by intracranial recordings, suggests that prior experience modulates early neural processing along a neural route initiated in an anterior system that includes OFG and TPO (Gamond et al., 2011). Moreover, TPO has been found to be involved in multiple skill learning processes, such as visual learning (Roland et al., 1990), auditory learning (Zhu et al., 2019), word learning (Elmer, Albrecht, Valizadeh, Francois, & Rodriguez-Fornells, 2018), and spatial learning (de Hoz et al., 2003). In this study, the FC between TPO and ACG was significantly correlated with individual lung nodule identification accuracy, which seems to suggest that learning to discriminate sophisticated visual features facilitated individual decision-making to identify lung tumors.

### 4.3 | Segregation between high-order and low-order brain functions

Our results elucidated that visual recognition experience prompted the disassociation between brain circuits for cognition and visual processing, such as between visual processing and attention control, and between visual processing and decision-making. Specifically, FC between the left LING and right MFG, between the left LING and right OFG, and between the left FFG and areas for decision-making, including ACGdor, SFG, and OFG were lower in the IR group.

The acquisition of visual expertise may involve the suppression of some preexisting neural representations and the development of new ones (Harley et al., 2009), which may help to filter out some nonrelevant information and thus facilitate more efficient task execution (Liu et al., 2020). In this study, we observed diminished functional synchronization between regions for visual processing (i.e., the left LING) and attention control (i.e., the MFG) in the IR group. MFG has been proposed as a junction of the dorsal and ventral attention networks, which acts as a circuit breaker to interrupt ongoing endogenous attention processes in the dorsal system and redirects attention to exogenous stimuli (Japee, Holiday, Satyshur, Mukai, & Ungerleider, 2015). MFG and LING have separate roles in visual object recognition: LING focuses more on lower-order visual information processing, while MFG focuses more on processing top-down information (Otsuka & Saiki, 2020). Furthermore, study on spatial sequences learning found that the left LING and right MFG works on discrete neural circuits (Nemmi, Boccia, Piccardi, Galati, & Guariglia, 2013), demonstrating their distinct roles again in visual information processing.

Moreover, the functional coupling between brain regions for visual processing (i.e., the left LING) and decision-making (i.e., the OFG) was lower in the IR group than the NC group. OFG is a member of the decision-making network that encodes expected outcomes and plays a critical role in flexible, outcome-guided behavior (Liu et al., 2020). Functional diverges between the OFG and left LING have been observed through categorization learning of visually similar objects (Xu, D'Lauro, Pyles, Kass, & Tarr, 2013). Moreover, it has been found that the activation of top-down projection of the OFG leads to response suppression in V1 during associative learning to filter out nonrelevant visual information to facilitate learning (Liu et al., 2020), again providing evidence that visual learning can induce suppression of some functional representations.

Furthermore, weakened FC was observed in the IR group between the left FFG and regions for decision-making (i.e., the ACGdor, SFG, and OFG). The general role of the left FFG in lower-order visual feature processing and visual learning has been demonstrated in numerous neuroimaging studies. Specifically, the left FFG was found to be engaged in the processing of abstract visual information (Devlin, Jamison, Gonnerman, & Matthews, 2006), its activity in radiologists could reliably distinguish between upright and inverted X-rays (Bilalic et al., 2016). Left FFG plays a vital role in visual categorization learning (Goold & Meng, 2017; Lech, Gunturkun, & Suchan, 2016); its activity was observed to be positively correlated with participants' perceptual performance (Bi, Chen, Zhou, He, & Fang, 2014; Liu et al., 2016; Mukai et al., 2007) and could be modulated by visual learning (Goold & Meng, 2017). The left FFG works for a different neural system involved in semantic category-based visual processes than ACG (Wei, Zhangi, Lyu, Hu, & Li, 2017), and was observed to have diverged function in contrast to the decision-making network through visual categorization learning for visually similar objects (Xu et al., 2013). Concretely, significant categorical discriminability has been observed in the ventral visual pathway (including the left FFG and left LING) during both early and late learning, whereas significant categorical discriminability in the prefrontal cortex is only present during early learning and disappears (as category familiarity increases) during late learning (Xu et al., 2013).

In addition, FCs between the left LING and MFG, between the left LING and OFG, and between the left FFG and regions for decision-making were negatively correlated with participants' lung nodule identification accuracy (Table 1). These results indicated the direct linkage between weakened FC of some brain regions and improved lung nodule identification performance. The process of lung nodule identification in X-ray images requires the collaborative work between multiple brain functional systems, and may involve filtering out task-irrelevant visual information. As skills develop, cognition and perception are developed separately (Duan et al., 2012). The resting-state brain activity is responsible for the coding of prior experience (Miall & Robertson, 2006), and the organization patterns of correlated spontaneous activity in resting states can be shaped by the coordinated activation of cortical networks during behaviors (Lewisa et al., 2009). We suggest that the diminished functional synchronization between the above functional systems in the IR group probably are the results of radiological diagnostic learning, which involves suppressing some existing neural representations between functional systems in order to achieve more effective domain-specific visual information processing.

### 4.4 | Limitations

We suggest several limitations be taken into consideration when interpreting the current findings. Firstly, in this study, the sample size is not optimal. The subjects were medical school students in rotation. There were about only 31 students, part of which were assigned to technical group. In this study, the homogeneity of radiological experience was carefully controlled. After rigorous behavioral screening procedure, we made sure that the participants with qualified behavioral performance were recruited. The sample size is the best we could possibly achieve. However, we do suggest that further studies with larger samples are encouraged to repeat the current findings. Second, the training duration for the experts is relatively short. The radiologist interns had to undertake rotations in MRI, B-scan ultrasonography, positron emission tomography-computed tomography (PET-CT) and X-ray departments within 4 months. One-month training in X-ray department is the longest for their training plan. After difficult negotiation with the hospital, we managed to align all the participants' training arrangement to starting from X-ray, but failed to increase the training duration. However, the total number of training cases for each participant was 763.0 ± 76.8 (Mean ± *SD*), which is sufficient to achieve the expertise (Annis & Palmeri, 2019). The results of behavioral test also supported this. We do suggest that further studies with a longer training duration conducted to repeat the current findings. Last but not least, a longitudinal experimental design and pretests for the participants were not carried out in this study. For cross-sectional studies, confounding factors such as congenital factors or long-term experiences in X-ray diagnosis before training, cannot be ruled out as possible explanations for the observed differences between groups. Although this is unlikely to happen, we should be careful to claim that the observed difference in FC is actually caused by short-term learning, or by congenital factors or long-term experiences. In further studies, longitudinal experiments should be considered to test our conclusions.

## 5 | CONCLUSIONS

The current study explored how real-world visual experience modulates connectivity patterns in resting-state brain activity using the model of radiologists. Region-wise functional connectivity analysis was performed based on functionally defined brain regions. Results suggested that visual expertise be accompanied by integration within or across brain circuits, and segregation between brain functions in the restful brain. The current study bridged the gap to understand the role of radiological visual experience on interregional spontaneous connectivity dynamics and may provide new ideas for understanding

the central mechanism of the formation of real-world visual recognition expertise. Our findings implied that radiographic visual recognition learning may modulate the plasticity of spontaneous brain functional interactions within or between brain functions, resulting in a neurological system for more efficient radiographic-specific visual information processing.

## ACKNOWLEDGMENTS

This article is supported by the National Natural Science Foundation of China (U19B2030, 61976167), Basic Scientific Research Program (No. JCKY2017204B102), the Science, Technology Projects of Xi'an, China (201809170CX11JC12), and Fundamental Research Funds for the Central Universities (No. JB191206). Also, we would like to thank Dr. Karen M. von Deneen for her professional service in language editing.

## CONFLICT OF INTEREST

The authors declare no conflict of interest.

## DATA AVAILABILITY STATEMENT

The data that support the findings of this study are available from the corresponding author upon reasonable request.

## ETHICS STATEMENT

This study was approved by the Ethics Committee of the First Affiliated Hospital of Xi'an Jiaotong University subcommittee on Human Studies and was conducted in accordance with the Declaration of Helsinki.

## ORCID

*Yue Wang* https://orcid.org/0000-0001-6170-6451
*Minghao Dong* https://orcid.org/0000-0002-0190-6985
*Jimin Liang* https://orcid.org/0000-0003-1428-5804

## REFERENCES

Alaerts, K., Swinnen, S., & Wenderoth, N. (2016). Sex differences in autism: A resting-state fMRI investigation of functional brain connectivity in males and females. *Social Cognitive and Affective Neuroscience*, *11*, 1002–1016. https://doi.org/10.1093/scan/nsw027

Allman, J., Hakeem, A., Erwin, J., Nimchinsky, E., & Hof, P. (2001). The anterior cingulate cortex: The evolution of an interface between emotion and cognition. *Unity of Knowledge: The Convergence of Natural and Human Science*, *935*, 107–117. https://doi.org/10.1111/j.1749-6632.2001.tb03476.x

Amad, A., Seidman, J., Draper, S., Bruchhage, M., Lowry, R., Wheeler, J., … Smith, M. (2017). Motor learning induces plasticity in the resting brain-drumming up a connection. *Cerebral Cortex*, *27*, 2010–2021. https://doi.org/10.1093/cercor/bhw048

Annis, J., & Palmeri, T. (2019). Modeling memory dynamics in visual expertise. *Journal of Experimental Psychology-Learning Memory and Cognition*, *45*, 1599–1618. https://doi.org/10.1037/xlm0000664

Bar, M. (2003). A cortical mechanism for triggering top-down facilitation in visual object recognition. *Journal of Cognitive Neuroscience*, *15*, 600–609. https://doi.org/10.1162/089892903321662976

Bi, T., Chen, J., Zhou, T., He, Y., & Fang, F. (2014). Function and structure of human left fusiform cortex are closely associated with perceptual learning of faces. *Current Biology*, *24*, 222–227. https://doi.org/10.1016/j.cub.2013.12.028

Bilalic, M., Grottenthaler, T., Naegele, T., & Lindig, T. (2016). The faces in radiological images: Fusiform face area supports radiological expertise. *Cerebral Cortex*, *26*, 1004–1014. https://doi.org/10.1093/cercor/bhu272

Bueicheku, E., Miro-Padilla, A., & Avila, C. (2019). Resting-state fMRI detects the effects of learning in short term: A visual search training study. *Human Brain Mapping*, *40*, 2787–2799. https://doi.org/10.1002/hbm.24560

Bush, G., Luu, P., & Posner, M. (2000). Cognitive and emotional influences in anterior cingulate cortex. *Trends in Cognitive Sciences*, *4*, 215–222. https://doi.org/10.1016/S1364-6613(00)01483-2

Cavanna, A., & Trimble, M. (2006). The precuneus: A review of its functional anatomy and behavioural correlates. *Brain*, *129*, 564–583. https://doi.org/10.1093/brain/awl004

Craddock, R., James, G., Holtzheimer, P., Hu, X., & Mayberg, H. (2012). A whole brain fMRI atlas generated via spatially constrained spectral clustering. *Human Brain Mapping*, *33*, 1914–1928. https://doi.org/10.1002/hbm.21333

de Hoz, L., Knox, J., & Morris, R. (2003). Longitudinal axis of the hippocampus: Both septal and temporal poles of the hippocampus support water maze spatial learning depending on the training protocol. *Hippocampus*, *13*, 587–603. https://doi.org/10.1002/hipo.10079

Devlin, J., Jamison, H., Gonnerman, L., & Matthews, P. (2006). The role of the posterior fusiform gyrus in reading. *Journal of Cognitive Neuroscience*, *18*, 911–922. https://doi.org/10.1162/jocn.2006.18.6.911

Dong, M., Qin, W., Zhao, L., Yang, X., Yuan, K., Zeng, F., … Tian, J. (2014). Expertise modulates local regional homogeneity of spontaneous brain activity in the resting brain: An fMRI study using the model of skilled acupuncturists. *Human Brain Mapping*, *35*, 1074–1084. https://doi.org/10.1002/hbm.22235

Dong, M., Li, J., Shi, X., Gao, S., Fu, S., Liu, Z., … Tian, J. (2015). Altered baseline brain activity in experts measured by amplitude of low frequency fluctuations (ALFF): A resting state fMRI study using expertise model of acupuncturists. *Frontiers in Human Neuroscience*, *9*, 99. https://doi.org/10.3389/fnhum.2015.00099

Donovan, T., & Litchfield, D. (2013). Looking for cancer: Expertise related differences in searching and decision making. *Applied Cognitive Psychology*, *27*, 43–49. https://doi.org/10.1002/acp.2869

Duan, X., He, S., Liao, W., Liang, D., Qiu, L., Wei, L., … Chen, H. (2012). Reduced caudate volume and enhanced striatal-DMN integration in chess experts. *NeuroImage*, *60*, 1280–1286. https://doi.org/10.1016/j.neuroimage.2012.01.047

Duchaine, B., & Nakayama, K. (2006). The Cambridge face memory test: Results for neurologically intact individuals and an investigation of its validity using inverted face stimuli and prosopagnosic participants. *Neuropsychologia*, *44*, 576–585. https://doi.org/10.1016/j.neuropsychologia.2005.07.001

Elmer, S., Albrecht, J., Valizadeh, S., Francois, C., & Rodriguez-Fornells, A. (2018). Theta coherence asymmetry in the dorsal stream of musicians facilitates word learning. *Scientific Reports*, *8*, 4565. https://doi.org/10.1038/s41598-018-22942-1

Evans, K. K., Cohen, M. A., Tambouret, R., Horowitz, T., Kreindel, E., & Wolfe, J. M. (2011). Does visual expertise improve visual recognition memory? *Attention, Perception, & Psychophysics*, *73*, 30–35. https://doi.org/10.3758/s13414-010-0022-5

Faul, F., Erdfelder, E., Lang, A. G., & Buchner, A. (2007). G*power 3: A flexible statistical power analysis program for the social, behavioral, and biomedical sciences. *Behavior Research Methods*, *39*, 175–191. https://doi.org/10.3758/BF03193146

Friedman, J., Hastie, T., & Tibshirani, R. (2008). Sparse inverse covariance estimation with the graphical lasso. *Biostatistics*, *9*, 432–441. https://doi.org/10.1093/biostatistics/kxm045

Friston, K., Ungerleider, L., Jezzard, P., & Turner, R. (1995). Characterizing modulatory interactions between areas VI and V2 in human cortex: A new treatment of functional MRI data. *Human Brain Mapping*, *2*, 211–224. https://doi.org/10.1002/hbm.460020403

Frith, U., & Frith, C. (2003). Development and neurophysiology of mentalizing. *Philosophical Transactions of the Royal Society B: Biological Sciences*, *358*, 459–473. https://doi.org/10.1098/rstb.2002.1218

Gamond, L., George, N., Lemarechal, J., Hugueville, L., Adam, C., & Tallon-Baudry, C. (2011). Early influence of prior experience on face perception. *NeuroImage*, *54*, 1415–1426. https://doi.org/10.1016/j.neuroimage.2010.08.08

Gold, J., & Shadlen, M. (2007). The neural basis of decision making. *Annual Review of Neuroscience*, *30*, 535–574. https://doi.org/10.1146/annurev.neuro.29.051605.113038

Goold, J., & Meng, M. (2017). Categorical learning revealed in activity pattern of left fusiform cortex. *Human Brain Mapping*, *38*, 3648–3658. https://doi.org/10.1002/hbm.23620

Grill-Spector, K., Kourtzi, Z., & Kanwisher, N. (2001). The lateral occipital complex and its role in object recognition. *Vision Research*, *41*, 1409–1422. https://doi.org/10.1016/S0042-6989(01)00073-6

Haller, S., & Radue, E. (2005). What is different about a radiologist's brain? *Radiology*, *236*, 983–989. https://doi.org/10.1148/radiol.2363041370

Harel, A. (2016). What is special about expertise? Visual expertise reveals the interactive nature of real-world object recognition. *Neuropsychologia*, *83*, 88–99. https://doi.org/10.1016/j.neuropsychologia.2015.06.004

Harel, A., Gilaie-Dotan, S., Malach, R., & Bentin, S. (2010). Top-down engagement modulates the neural expressions of visual expertise. *Cerebral Cortex*, *20*, 2304–2318. https://doi.org/10.1093/cercor/bhp316

Harel, A., Kravitz, D., & Baker, C. (2013). Beyond perceptual expertise: Revisiting the neural substrates of expert object recognition. *Frontiers in Human Neuroscience*, *7*, 885. https://doi.org/10.3389/fnhum.2013.00885

Harley, E., Pope, W., Villablanca, J., Mumford, J., Suh, R., Mazziotta, J., … Engel, S. (2009). Engagement of fusiform cortex and disengagement of lateral occipital cortex in the acquisition of radiological expertise. *Cerebral Cortex*, *19*, 2746–2754. https://doi.org/10.1093/cercor/bhp051

Humphreys, G., Price, C., & Riddoch, J. (1999). From objects to names: A cognitive neuroscience approach. *Psychological Research*, *62*, 118–130. https://doi.org/10.1007/s004260050046

Japee, S., Holiday, K., Satyshur, M., Mukai, I., & Ungerleider, L. (2015). A role of right middle frontal gyrus in reorienting of attention: A case study. *Frontiers in Systems Neuroscience*, *9*, 23. https://doi.org/10.3389/fnsys.2015.00023

Ji, H., Chen, B., Petro, N., Yuan, Z., Zheng, N., & Keil, A. (2019). Functional source separation for EEG-fMRI fusion: Application to steady-state visual evoked potentials. *Frontiers in Neurorobotics*, *13*, 24. https://doi.org/10.3389/fnbot.2019.00024

Kawashima, R., Roland, P., & O'Sullivan, B. (1995). Functional anatomy of reaching and visuomotor learning: A positron emission tomography study. *Cerebral Cortex (New York, N.Y.: 1991)*, *5*, 111–122. https://doi.org/10.1093/cercor/5.2.111

Kelly, A., & Garavan, H. (2005). Human functional neuroimaging of brain changes associated with practice. *Cerebral Cortex*, *15*, 1089–1102. https://doi.org/10.1093/cercor/bhi005

Kundel, H. L., Nodine, C. F., Conant, E. F., & Weinstein, S. P. (2007). Holistic component of image perception in mammogram interpretation: Gaze-tracking study. *Radiology*, *242*, 396–402. https://doi.org/10.1148/radiol.2422051997

LaConte, S., Anderson, J., Muley, S., Ashe, J., Frutiger, S., Rehm, K., … Strother, S. (2003). The evaluation of preprocessing choices in single-subject BOLD fMRI using NPAIRS performance metrics. *NeuroImage*, *18*, 10–27. https://doi.org/10.1006/nimg.2002.1300

Lech, R., Gunturkun, O., & Suchan, B. (2016). An interplay of fusiform gyrus and hippocampus enables prototype and exemplar-based category learning. *Behavioural Brain Research*, *311*, 239–246. https://doi.org/10.1016/j.bbr.2016.05.049

Ledoit, O., & Wolf, M. (2004). A well-conditioned estimator for largedimensional covariance matrices. *Journal of Multivariate Analysis*, *88*, 365–411. https://doi.org/10.1016/S0047-259X(03)00096-4

Lee, D., Rushworth, M., Walton, M., Watanabe, M., & Sakagami, M. (2007). Functional specialization of the primate frontal cortex during decision making. *Journal of Neuroscience*, *27*, 8170–8173. https://doi.org/10.1523/JNEUROSCI.1561-07.2007

Lewisa, C., Baldassarre, A., Committeri, G., Romani, G., & Corbetta, M. (2009). From the cover: Learning sculpts the spontaneous activity of the resting human brain. *Proceedings of the National Academy of Sciences of the United States of America*, *106*, 17558–17563. https://doi.org/10.1073/pnas.0902455106

Lin, P., Hasson, U., Jovicich, J., & Robinson, S. (2011). A neuronal basis for task-negative responses in the human brain. *Cerebral Cortex*, *21*, 821–830. https://doi.org/10.1093/cercor/bhq151

Liu, D., Deng, J., Zhang, Z., Zhang, Z., Sun, Y., Yang, T., & Yao, H. (2020). Orbitofrontal control of visual cortex gain promotes visual associative learning. *Nature Communications*, *11*, 2784–2797. https://doi.org/10.1038/s41467-020-16609-7

Liu, Z., Zhou, Q., Zhang, M., Shi, Q., Liu, X., Chen, R., … Sui, G. (2016). Perceptual learning: A novel method to improve the near reading abilities in early stage presbyopia patients. *International Journal of Clinical and Experimental Medicine*, *9*, 12249–12255.

Machielsen, W., Rombouts, S., Barkhof, F., Scheltens, P., & Witter, M. (2000). fMRI of visual encoding: Reproducibility of activation. *Human Brain Mapping*, *9*, 156–164. https://doi.org/10.1002/(SICI)1097-0193(200003)9:3<156::AID-HBM4>3.0.CO;2-Q

Maguire, E., Frith, C., & Morris, R. (1999). The functional neuroanatomy of comprehension and memory: The importance of prior knowledge. *Brain*, *122*, 1839–1850. https://doi.org/10.1093/brain/122.10.1839

Marcotte, K., & Ansaldo, A. (2014). Age-related behavioural and neurofunctional patterns of second language word learning: Different ways of being successful. *Brain and Language*, *135*, 9–19. https://doi.org/10.1016/j.bandl.2014.04.004

Martens, F., Bulthe, J., van Vliet, C., & Op de Beeck, H. (2018). Domain-general and domain-specific neural changes underlying visual expertise. *NeuroImage*, *169*, 80–93. https://doi.org/10.1016/j.neuroimage.2017.12.013

McGugin, R., Gatenby, J., Gore, J., & Gauthier, I. (2012). High-resolution imaging of expertise reveals reliable object selectivity in the fusiform face area related to perceptual performance. *Proceedings of the National Academy of Sciences of the United States of America*, *109*, 17063–17068. https://doi.org/10.1073/pnas.1116333109

Melo, M., Scarpin, D., Amaro, E., Passos, R., Sato, J., Friston, K., & Price, C. (2011). How doctors generate diagnostic hypotheses: A study of radiological diagnosis with functional magnetic resonance imaging. *PLoS One*, *6*, e28752. https://doi.org/10.1371/journal.pone.0028752

Metz, C. (2006). Receiver operating characteristic analysis: A tool for the quantitative evaluation of observer performance and imaging systems. *Journal of the American College of Radiology*, *3*, 413–422. https://doi.org/10.1016/j.jacr.2006.02.021

Miall, R., & Robertson, E. (2006). Functional imaging: Is the resting brain resting? *Current Biology*, *16*, R998–R1000. https://doi.org/10.1016/j.cub.2006.10.041

Miller, E. (2000). The prefrontal cortex and cognitive control. *Nature Reviews Neuroscience*, *1*, 59–65. https://doi.org/10.1038/35036228

Mukai, I., Kim, D., Fukunaga, M., Japee, S., Marrett, S., & Ungerleider, L. (2007). Activations in visual and attention-related areas predict and correlate with the degree of perceptual learning. *Journal of Neuroscience*, *27*, 11401–11411. https://doi.org/10.1523/JNEUROSCI.3002-07.2007

Myles-Worsley, M., Johnston, W. A., & Simons, M. A. (1998). The influence of expertise on X-ray image processing. *Journal of Experimental Psychology: Learning, Memory, and Cognition*, *14*, 553–557. https://doi.org/10.1037/0278-7393.14.3.553

Nakamura, K., Kawashima, R., Sato, N., Nakamura, A., Sugiura, M., Kato, T., … Zilles, K. (2000). Functional delineation of the human occipito-temporal areas related to face and scene processing: A PET study. *Brain*, *123*, 1903–1912. https://doi.org/10.1093/brain/123.9.1903

Nakamura, K., Kawashima, R., Sugiura, M., Kato, T., Nakamura, A., Hatano, K., … Kojima, S. (2001). Neural substrates for recognition of familiar voices: A PET study. *Neuropsychologia*, *39*, 1047–1054. https://doi.org/10.1016/S0028-3932(01)00037-9

Nemmi, F., Boccia, M., Piccardi, L., Galati, G., & Guariglia, C. (2013). Segregation of neural circuits involved in spatial learning in reaching and navigational space. *Neuropsychologia*, *51*, 1561–1570. https://doi.org/10.1016/j.neuropsychologia.2013.03.031

Neumann, N., Lotze, M., & Eickhoff, S. (2016). Cognitive expertise: An ALE meta-analysis. *Human Brain Mapping*, *37*, 262–272. https://doi.org/10.1002/hbm.23028

Nguyen, X., Epps, J., & Bailey, J. (2010). Information theoretic measures for clusterings comparison: Is a correction for chance necessary? *Journal of Machine Learning Research*, *11*, 2837–2854. https://doi.org/10.1007/s10846-010-9415-x

Nieuwenhuis, S., Riddeerinkhof, K. R., Blow, J., Band, G. P. H., & Kok, A. (2001). Error-related brain potentials are differentially related to awareness of response errors: Evidence from an antisaccade task. *Psychophysiology*, *38*, 752–760. https://doi.org/10.1017/S0048577201001111

Niu, H., Li, H., Sun, L., Su, Y., Huang, J., & Song, Y. (2014). Visual learning alters the spontaneous activity of the resting human brain: An fNIRS study. *Biomed Research International*, *2014*, 631425. https://doi.org/10.1155/2014/631425

Nodine, C. F., Kundel, H. L., Lauver, S. C., & Toto, L. C. (1996). Nature of expertise in searching mammograms for breast masses. *Academic Radiology*, *3*, 1000–1006. https://doi.org/10.1016/S1076-6332(96)80032-8

Nodine, C. F., Mello-Thoms, C., Kundel, H. L., & Weinstein, S. P. (2002). Time course of perception and decision making during mammographic interpretation. *American Journal of Roentgenology*, *179*, 917–923. https://doi.org/10.2214/ajr.179.4.1790917

Otsuka, S., & Saiki, J. (2020). Neural mechanisms of memory enhancement and impairment induced by visual statistical learning. *Journal of Cognitive Neuroscience*, *32*, 1749–1763. https://doi.org/10.1162/jocn_a_01589

Parisot, S., Arslan, S., Passerat-Palmbach, J., Wells, W. M., & Rueckert, D. (2016). Group-wise parcellation of the cortex through multiscale spectral clustering. *NeuroImage*, *136*, 68–83. https://doi.org/10.1016/j.neuroimage.2016.05.035

Patel, R., Borsook, D., & Becerra, L. (2008). Modulation of resting state functional connectivity of the brain by naloxone infusion. *Brain Imaging and Behavior*, *2*, 11–20. https://doi.org/10.1007/s11682-007-9011-2

Paus, T. (2001). Primate anterior cingulate cortex: Where motor control, drive and cognition interface. *Nature Reviews Neuroscience*, *2*, 417–424. https://doi.org/10.1109/96.496036

Pavlovic, D., Pavlovic, A., & Lackovic, M. (2009). The anterior cingulate cortex. *Archives of Biological Sciences*, *61*, 659–673. https://doi.org/10.2298/ABS0904659P

Peter, R. (1987). Silhouettes: A graphical aid to the interpretation and validation of cluster analysis. *Journal of Computational & Applied Mathematics*, *20*, 53–65. https://doi.org/10.1016/0377-0427(87)90125-7

Posner, M., & Digirolamo, G. (1998). Executive attention conflict, target detection, and cognitive control. In R. Parasuraman (Ed.), *The Attentive Brain* (pp. 401–423). Cambridge, MA: The MIT Press.

Posner, M., & Raichle, M. (1995). Images of mind. *Quarterly Review of Biology*, *18*, 327–383.

Roelofs, A., van Turennout, M., & Coles, M. (2006). Anterior cingulate cortex activity can be independent of response conflict in Stroop-like tasks. *Proceedings of the National Academy of Sciences of the United States of America*, *103*, 13884–13889. https://doi.org/10.1073/pnas.0606265103

Roland, P., Gulyas, B., Seitz, R., Bohm, C., & Stone-Elander, S. (1990). Functional anatomy of storage, recall, and recognition of a visual pattern in man. *Neuroreport*, *1*, 53–56. https://doi.org/10.1097/00001756-199009000-00015

Rourke, L., Cruikshank, L. C., Shapke, L., & Singhal, A. (2016). A neural marker of medical visual expertise: Implications for training. *Advances in Health Sciences Education*, *21*, 953–966. https://doi.org/10.1007/s10459-016-9712-7

Samei, E., Krupinski, E., & Hendee, W. (2010). The handbook of medical image perception and techniques. *Medical Physics*, *37*, 6112. https://doi.org/10.1118/1.3505328

Shen, X., Tokoglu, F., Papademetris, X., & Constable, R. (2013). Groupwise whole-brain parcellation from resting-state fMRI data for network node identification. *NeuroImage*, *82*, 403–415. https://doi.org/10.1016/j.neuroimage.2013.05.081

Song, G., Qiu, J., Li, C., Li, J., Gui, S., Zhu, H., & Zhang, Y. (2017). Alterations of regional homogeneity and functional connectivity in pituitary adenoma patients with visual impairment. *Scientific Reports*, *7*, 13074. https://doi.org/10.1038/s41598-017-13214-5

Thirion, B., Varoquaux, G., Dohmatob, E., & Poline, J. (2014). Which fMRI clustering gives good brain parcellations? *Frontiers in Neuroscience*, *8*, 167. https://doi.org/10.3389/fnins.2014.00167

Tzourio-Mazoyer, N., Landeau, B., Papathanassiou, D., Crivello, F., Etard, O., Delcroix, N., … Joliot, M. (2002). Automated anatomical labeling of activations in SPM using a macroscopic anatomical parcellation of the MNI MRI single-subject brain. *NeuroImage*, *15*, 273–289. https://doi.org/10.1006/nimg.2001.0978

Ungerleider, L., & Haxby, J. (1994). 'What' and 'where' in the human brain. *Current Opinion in Neurobiology*, *4*, 157–165. https://doi.org/10.1016/0959-4388(94)90066-3

Urner, M., Schwarzkopf, D., Friston, K., & Rees, G. (2013). Early visual learning induces long-lasting connectivity changes during rest in the human brain. *NeuroImage*, *77*, 148–156. https://doi.org/10.1016/j.neuroimage.2013.03.050

van den Heuvel, M., Mandl, R., & Pol, H. (2008). Normalized cut group clustering of resting-state fMRI data. *PLoS One*, *3*, e2001. https://doi.org/10.1371/journal.pone.0002001

Vandenberghe, R., Price, C., Wise, R., Josephs, O., & Frackowiak, R. (1996). Functional anatomy of a common semantic system for words and pictures. *Nature*, *383*, 254–256. https://doi.org/10.1038/383254a0

Vandenberghe, R., Nobre, A., & Price, C. (2002). The response of left temporal cortex to sentences. *Journal of Cognitive Neuroscience*, *14*, 550–560. https://doi.org/10.1162/08989290260045800

Varoquaux, G., & Craddock, R. (2013). Learning and comparing functional connectomes across subjects. *NeuroImage*, *80*, 405–415. https://doi.org/10.1016/j.neuroimage.2013.04.007

Varoquaux, G., Baronnet, F., Kleinschmidt, A., Fillard, P., & Thirion, B. (2010). Detection of brain functional-connectivity difference in post-stroke patients using group-level covariance modeling. *Medical Image Computing and Computer-Assisted Intervention*, *13*, 200–208. doi: https://doi.org/10.1007/978-3-642-15705-9_25

Varoquaux, G., Gramfort, A., Poline, J. B., & Thirion, B. (2010). Brain covariance selection: Better individual functional connectivity models using population prior. *Advances in Neural Information Processing Systems*, *23*, 2334–2342.

Vila-Maldonado, S., Abellán, J., Sáez-Gallego, N., García-López, L., & Contreras, O. (2014). Decision-making and visual perception skills in

youth volleyball players and non-players. *Journal of Sport and Health Research*, *6*, 265–276.

Vogt, B., & Derbyshire, S. (2009). Visceral circuits and cingulate-mediated autonomic functions. In B. A. Vogt (Ed.), *Cingulate neurobiology and disease* (pp. 220–235). Oxford, NY: Oxford University Press.

Wagner, A., Shannon, B., Kahn, I., & Buckner, R. (2005). Parietal lobe contributions to episodic memory retrieval. *Trends in Cognitive Sciences*, *9*, 445–453. https://doi.org/10.1016/j.tics.2005.07.001

Waite, S., Farooq, Z., Grigorian, A., Sistrom, C., Kolla, S., & Mancuso, A. (2020). A review of perceptual expertise in radiology: How it develops, how we can test it, and why humans still matter in the era of artificial intelligence. *Academic Radiology*, *27*, 26–38. https://doi.org/10.1016/j.acra.2019.08.018

Wallis, G., & Bulthoff, H. (1999). Learning to recognize objects. *Trends in Cognitive Sciences*, *3*, 22–31. https://doi.org/10.1016/S1364-6613(98)01261-3

Wang, J., & Wang, H. (2016). A Supervoxel-based method for Groupwise whole brain parcellation with resting state fMRI data. *Frontiers in Human Neuroscience*, *10*, 659. https://doi.org/10.3389/fnhum.2016.00659

Wang, R., Zhang, J., Klein, S., Levi, D., & Yu, C. (2014). Task relevancy and demand modulate double-training enabled transfer of perceptual learning. *Vision Research*, *61*, 33–38. https://doi.org/10.1016/j.visres.2011.07.019

Wang, X., Peelen, M., Han, Z., He, C., Caramazza, A., & Bi, Y. (2015). How visual is the visual cortex? Comparing connectional and functional fingerprints between congenitally blind and sighted individuals. *Journal of Neuroscience*, *35*, 12545–12559. https://doi.org/10.1523/JNEUROSCI.3914-14.2015

Wei, L., Zhangi, X., Lyu, C., Hu, S., & Li, Z. (2017). Brain activation of semantic category-based grouping in multiple identity tracking task. *PLoS One*, *12*, e0177709. https://doi.org/10.1371/journal.pone.0177709

Wenderoth, N., Debaere, F., Sunaert, S., & Swinnen, S. (2015). The role of anterior cingulate cortex and precuneus in the coordination of motor behaviour. *European Journal of Neuroscience*, *22*, 235–246. https://doi.org/10.1111/j.1460-9568.2005.04176.x

Xiao, L., Zhang, J., Wang, R., Klein, S., Levi, D., & Yu, C. (2008). Complete transfer of perceptual learning across retinal locations enabled by double training. *Current Biology*, *18*, 1922–1926. https://doi.org/10.1016/j.cub.2008.10.030

Xu, Y., D'Lauro, C., Pyles, J., Kass, R., & Tarr, M. (2013). Fine-grained temporal coding of visually-similar categories in the ventral visual pathway and prefrontal cortex. *Frontiers in Psychology*, *4*, 684. https://doi.org/10.3389/fpsyg.2013.00684

Zhu, B., Chen, C., Shao, X., Liu, W., Ye, Z., Zhuang, L., … Xue, G. (2019). Multiple interactive memory representations underlie the induction of false memory. *Proceedings of the National Academy of Sciences of the United States of America*, *116*, 3466–3475. https://doi.org/10.1073/pnas.1817925116

## SUPPORTING INFORMATION

Additional supporting information may be found online in the Supporting Information section at the end of this article.

**How to cite this article:** Wang, Y., Jin, C., Yin, Z., Wang, H., Ji, M., Dong, M., & Liang, J. (2021). Visual experience modulates whole-brain connectivity dynamics: A resting-state fMRI study using the model of radiologists. *Human Brain Mapping*, *42*(14), 4538–4554. https://doi.org/10.1002/hbm.25563